Journal of ELECTRONIC MATERIALS, Vol. 50, No. 6, 2021
https://doi.org/10.1007/s11664-021-08816-9

ORIGINAL RESEARCH ARTICLE

Facile Synthesis of Fe_3O_4/ZnO Nanocomposite: Applications to Photocatalytic and Antibacterial Activities

M. SHAHSANK,[1] H.S. BHOJYA NAIK ,[1,6] G. NAGARAJU,[2] RANGAPPA S. KERI,[3] M. MADHUKARA NAIK,[4] and K. LINGARAJU[5]

1.—Department of Studies and Research in Industrial Chemistry, School of Chemical Sciences, Kuvempu University, Shankaragatta 577451, India. 2.—Energy Materials Research Laboratory, Department of Chemistry, Siddaganga Institute of Technology, Tumakuru 572 103, India. 3.—Center for Nano and Material Sciences, Jain University, Jain Global Campus, Jakkasandra Post, Kanakapura Road, Ramanagara District, Karnataka 562112, India. 4.—Department of Chemistry, MVJ College of Engineering, Bengaluru, Karnataka 560 067, India. 5.—Department of Studies and Research in Environmental Science, Tumkur University, Tumkur, Karnataka 572103, India. 6.—e-mail: hsb_naik@rediffmail.com

In the current work, we have reported the preparation of Fe_3O_4/ZnO nanocomposite (NC) via co-precipitation. The prepared Fe_3O_4/ZnO nanocomposite were characterized by x-ray diffraction, Fourier transform infrared (FT-IR) spectroscopy, scanning electron microscopy (SEM) equipped with energy dispersive x-ray analysis (EDAX), transmission electron microscopy (TEM), Brunauer–Emmett–Teller (BET) surface area analysis, ultraviolet-diffuse reflectance spectroscopy (UV-DRS) and photoluminescence spectroscopy (PL). From the x-ray diffraction pattern, the average crystallite size of Fe_3O_4/ZnO NC was found to be 13 nm. UV-DRS showed an energy band gap of 2.3 eV for the prepared sample. From the Brunauer–Emmett–Teller (BET) surface area analysis, total pore volume (V_P) and mean pore diameter (r_p) were found to be 12.647 m^2g^{-1}, 0.024125 cm^3g^{-1} and 7.6302 nm. The functional groups and metal to oxygen bonding in Fe_3O_4/ZnO NC were observed in FT-IR. SEM and TEM micrograph of Fe_3O_4/ZnO NC show flake- and grain-like structures, and the luminescence spectrum shows blue emission. The photocatalytic activity of Fe_3O_4/ZnO NC was examined using industrial effluent dyes such as Evans blue (90% in 150 min) and Rhodamine B (RB) (99% in 150 min) under UV light irradiation. Further, Fe_3O_4/ZnO NC also showed a superior zone of inhibition against pathogenic bacterial strains such as *Escherichia coli* and *Staphylococcus aureus* by agar well diffusion compared to Fe_3O_4 and ZnO nanoparticles.

Key words: Fe_3O_4, ZnO nanocomposite, BET, photodegradation, antibacterial activity

INTRODUCTION

In recent years, the development of industries has increased pollution. Methylene blue, Evans blue, remazol red, malachite green, methyl orange etc., are colored dyes used in textile industries which leads to contamination of environmental resources (global warming, ozone layer depletion, etc.), and it also harms aquatic life and humans[1] (skin diseases, lung infections, etc.). Photocatalytic degradation is one of the most effective strategies to reduce the contamination from industrial waste.

Metal oxides such as TiO_2, ZnO, ZrO_2, SnO_2 and Fe_3O_4 are largely used in the degradation process.[2] Among them, semiconductor ZnO is preferred as the photocatalyst due to its high photocatalytic activity,

(Received August 10, 2020; accepted February 12, 2021; published online March 30, 2021)

wide band gap, high quantum efficiency, and low cost.[3] Magnetic core-shell nanoparticles have been used to improve the photocatalytic degradation property. Among several, Fe_3O_4 has important magnetic properties, low cost, chemical stability, mechanical hardness, easy separation, is non-toxic, and in the octahedral site there is a shift of electrons between Fe^{2+} and Fe^{3+} oxidation states. There are many physical and chemical methods, such as hydrothermal, co-precipitation, and sol-gel, for the synthesis of magnetic nanoparticles but co-precipitation is the most well-known synthesis route to achieve good morphology and enhanced properties.[4]

Several NPs inhibit the growth of bacteria by representing strong antibacterial properties which act against *Staphylococcus aureus* and *Escherichia coli* bacteria.[5] Nowadays, metal oxide NC has shown fascinating properties and enormous applications within the fields of biology, medicine, sensors and the environment. Jilla et al. prepared an agglomerated Fe_3O_4/ZnO nanocomposite by free surface sonication and its application in photocatalytic degradation of dye.[6] The visible light photocatalytic application of Fe_3O_4@LPH@Ag/Ag_3PO_4 sub microspheres was synthesized by Chao et al., where Fe_3O_4@LDH was prepared by a hydrothermal method and Fe_3O_4@LDH@PO_4^{3-} by ion exchange.[7] Sobia et al. prepared a microsphere Fe_3O_4@MIL-100(Fe) core-shell for photocatalytic degradation by a hydrothermal method.[8] Jian et al. synthesized Fe_3O_4@ZnO nanospheres by a chemical method for photocatalytic and antibacterial activity.[9] Agglomerated Fe_3O_4@MOR@CuO was prepared by Rajablet al., who used a hydrothermal method for a visible light driven photocatalyst.[10] An Fe_3O_4@ZnO core-shell was prepared by Jian Wang et al. by co-precipitation for the photocatalytic property.[9]

In this current work, Fe_3O_4/ZnO nanocomposites have been synthesized by a simple co-precipitation method and its structural, optical, morphological, photocatalytic and antibacterial properties are studied.

EXPERIMENTAL

Preparation of Fe_3O_4/ZnO Nanocomposite

Analytical grade reagents were purchased from Fluka, Sigma-Aldrich and Acros and used as supplied. The preparation of Fe_3O_4/ZnO NC involves two steps.

Step I: Preparation of Fe_3O_4

$FeCl_3.6H_2O$ (9.4 g) and $FeCl_2.4H_2O$ (3.46 g) were dissolved in 100 mL of double distilled water in a round bottom flask at 70–80°C for 30 min. Then the solution was heated in a pre-heated oil bath at 85°C by stirring until the solution turned yellow. After 30 min, 20 mL NH_4OH was added dropwise into the solution. The reaction mixture was then left in the heated oil bath for 30 min. Once the reaction was completed, the reaction mixture was removed from the oil bath and cooled. Then the prepared magnetic nanoparticles were washed with double distilled water until neutral pH was reached from basic medium and further washed with methanol (30 mL). The obtained black powder of Fe_3O_4 NPs was vacuum dried and stored.

Step II: Preparation of Fe_3O_4/ZnO Nanocomposite

The Fe_3O_4/ZnO NC was attained by later deposition of ZnO on the surface of iron nanoparticles through thermal decomposition. Fifty milliliters of ethyl alcohol was added to the mixture of 0.49 g of Fe_3O_4 NPs and 3.93 g of $Zn(CH_3COO)_2.4H_2O$. The mixture was stirred at 70°C for 1 h. Dropwise addition of 1.58 mL of diethanol amine and 5 mL of ethyl alcohol was done under stirring until a dark brown colour was obtained. Stirring was continued for 2 h until the solution turned to a gel. Fe_3O_4/ZnO NC was then collected by simple magnetic decantation and ultimately washed with water (40 mL) and methanol (40 mL×4) then dried under vacuum at 90°C for 24 h (Scheme 1).[11]

Characterization

Powder x-ray diffraction (XRD) of prepared Fe_3O_4/ZnO NC was used to observe the crystalline phases using a Rigaku Ultima-IV x-ray diffractometer using Cu-Kα radiation (λ = 1.5406 Å). FTIR spectra were recorded by a Bruker spectrophotometer using KBr pellets. TLC silica gel 60 F_{254} (Merck) detected UV light (254 nm) and iodine vapors. Scanning electron microscope (SEM) analysis was done using a JEOL-JSM 7100F, and transmission electron microscopy (TEM) was done by a JEOL-JEM 2100. The surface area and pore size distribution was studied by Brunauer–Emmett–Teller (BET) using a Belsorp Max instrument (Japan). Photoluminescence studies (PL) were carried out using an Agilent Technologies Cary-60 Eclipse spectrophotometer.

Photocatalytic Setup

The photoreactor assembly includes a cylindrical tube, the inside of which is made transparent to irradiate the light. A tungsten vapour lamp (300 W) of medium pressure was placed at the centre of the system and cooling jacket was used for refrigeration. Fans were afixed to the four corners of the photoreactor in order to cool the reactor. As the lamp produces heat, continuous circulation of cold water through the cooling jacket is maintained. A set of quartz tubes of 100 mL capacity were placed around the lamp and filled with organic pollutants. Using an air pump, bubbling of the solution was maintained in order to distribute the catalyst uniformly.

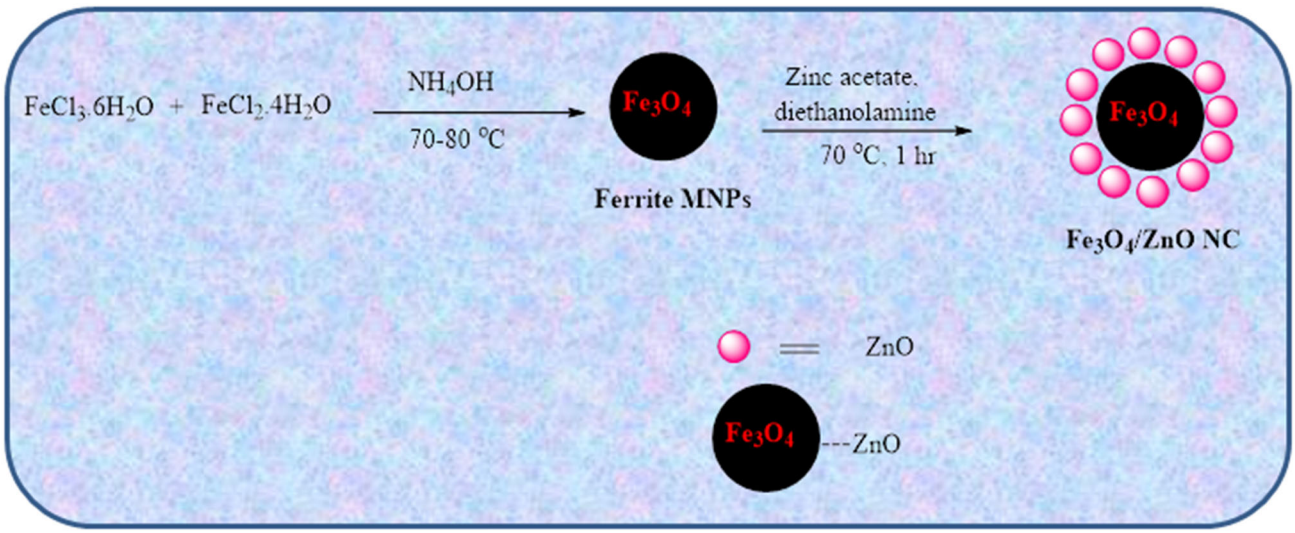

Scheme 1. Synthesis of Fe_3O_4/ZnO NC.

Photocatalytic Activity

The photocatalytic property of the Fe_3O_4/ZnO NC was examined by the photodegradation of Evans blue (EB) and Rhodamine B (RB) dye aqueous solution under UV light illumination. Fifty milligrams of the catalyst (Fe_3O_4, ZnO, Fe_3O_4/ZnO NC) was added to different glass tubes containing 5 ppm of two different dyes (three tubes for each dye). After mixing, the solution was kept in the dark and air bubbled for 30 min to obtain the adsorption/desorption equilibrium between the photocatalyst and dye before illumination. After attaining equilibrium, UV light was focused on the solution with the circulation water. At 30-min intervals, 4 mL of the solution was taken out and used to test the absorbance. An Agilent Technologies Cary-60 UV-Visible spectrophotometer was used.

The percentage degradation of the dye was calculated using the following relation.

$$\eta = [(c_0 - c_t)/c_0] \times 100\% \quad (1)$$

where η is the percentage of degradation, the initial concentration of the dye is given by c_0 and the concentration of the dye after irradiation is given by c_t.[12]

Evaluation of Antibacterial Activity

ZnO, Fe_3O_4 and Fe_3O_4/ZnO NC were examined for antibacterial activity by Agar well diffusion[13,14] against gram negative bacteria—*Escherichia coli* [NCIM-5051] and gram positive bacterial strains *Staphylococcus aureus* [NCIM-5022] were sub-cultured in sterile nutrient agar medium and poured into sterile petri dishes for solidifying. Using a sterilized L-shaped glass rod, matured broth culture of individual pathogenic bacterial strains was spread uniformly over the surface of agar plates using a sterile cork borer. In each individual agar plate about 6-mm wells were made. Different concentrations of ZnO, Fe_3O_4, Fe_3O_4/ZnO NC (150, 300 and 450 μg/well) were dispersed in sterile distilled water and dispersed into the well using micropipettes. For positive control, a standard antibiotic (ciprofloxacin) was used. The zone of inhibition of

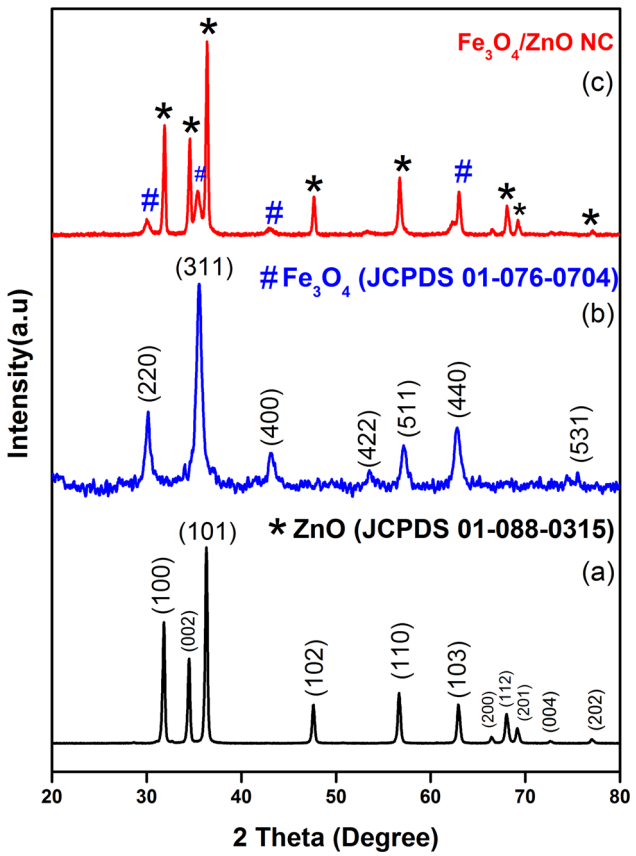

Fig. 1. XRD patterns of Fe_3O_4/ZnO NC.

each well was measured once the plates were incubated at 37°C for 24 h.

RESULT AND DISCUSSION

XRD Studies

The XRD patterns of ZnO, Fe_3O_4, and Fe_3O_4/ZnO NC are shown in Fig. 1a, b, and c. Six characteristic peaks for Fe_3O_4 NPs (2θ = 30.16°, 35.48°, 43.13°, 53.49°, 56.91° and 62.71°) are marked by their indices (220), (311), (400), (422), (511) and (440), respectively. These peaks are well indexed to the JCPDS card no. 01-076-0704. The eight peaks for ZnO NPs (2θ = 31.84°, 34.52°, 36.33°, 47.63°, 56.71°, 62.96°, 68.13°, 69.18°) are marked by their indices (100), (002), (101), (102), (110), (103), (112) and (201) with JCPDS card no. (01-088-0315). The XRD pattern of Fe_3O_4/ZnO nanocomposite confirmed the presence of Fe_3O_4 NPs and ZnO NPs combined together which formed a composite. The marking of peaks with * (ZnO) and # (Fe_3O_4) can be observed in the Fe_3O_4/ZnO NC without any additional impurities. Hence, no extra peaks were absorbed which confirmed that Fe_3O_4 nanoparticles were coated with ZnO.[9,14]

FTIR Studies

The prepared Fe_3O_4/ZnO NC were characterized by FTIR and are shown in Fig. 2. The strong absorption band at 450 cm^{-1} is due to the different stretching modes of the Zn-O bonding in zinc oxide. The stretching vibrations of the Fe-O bonding fall near to each other at 563 cm^{-1}. Furthermore, the peak at 1607 cm^{-1} shows the C-H bending vibration and the C-O stretching vibration attributed to 1102 cm^{-1} and 1409 cm^{-1}. This confirms that all the characteristic peaks of Fe_3O_4 and ZnO are present in Fe_3O_4/ZnO NC. Because of the increased concentration of ZnO in the Fe_3O_4/ZnO NC system, a broad band is observed between 450 (υ_1) and 557 (υ_2) cm^{-1} which is attributed to the Zn-O vibrations. This increased concentration of ZnO makes resolution of the υ_1 and υ_2 peaks difficult. However, a peak is observed around 563 cm^{-1} which can be attributed to the vibrations between oxygen and iron. The strong absorption peak at 3425 cm^{-1} shows the O-H stretching vibration. The absorption peaks at 2914 cm^{-1} are attributed to the C-H stretching vibrations of the -CH_2 functional group.[15]

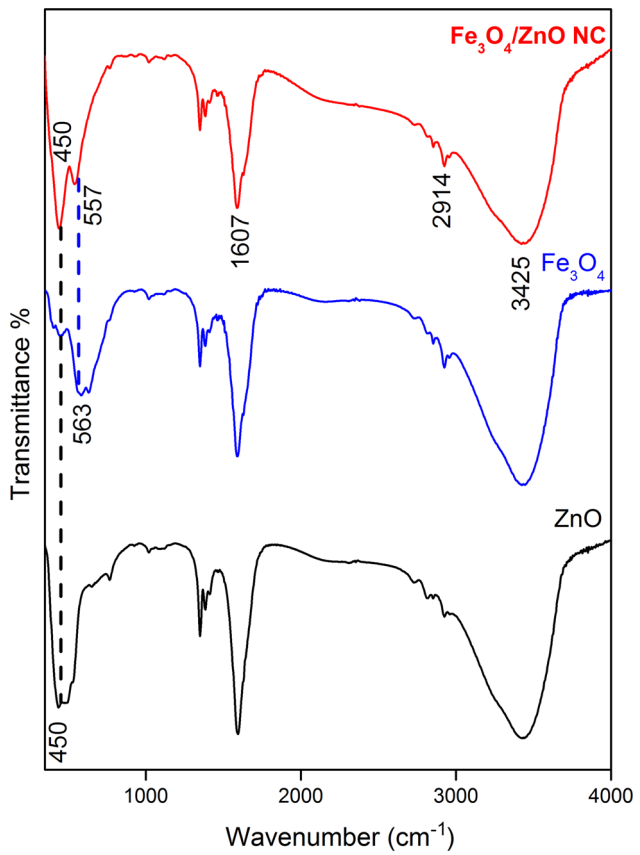

Fig. 2. FTIR spectra of ZnO, Fe_3O_4, and Fe_3O_4/ZnO NC.

Morphological Studies

Figure 3a and b shows the SEM images of Fe_3O_4 and ZnO. From analysis of SEM micrographs, almost uniform-sized particles with flake- and grain-like structure were observed and conjointly marked tendency to make giant clusters. Further, Fig. 3c and d indicates the composite structure of ZnO and Fe_3O_4 magnetic nanoparticles. Figure 4 shows the EDAX of Fe_3O_4/ZnO NC. From EDAX, iron, zinc and oxygen peaks (Pt is excluded as it from platinised carbon tape) clearly confirm the presence of Fe_3O_4 and ZnO in the prepared nanocomposite.[16]

HRTEM with SAED Analysis

Figure 5a, b, c, and d clearly represents the TEM images of Fe_3O_4/ZnO NC and the overall size and structure of the prepared nanocomposite. We can also identify the spherical and hexagonal nanoflakes forming the clusters by combining each other having low dispersion which tends to the magnetic property of the synthesized nanocomposite.[17,18] During electron irradiation there is difference in electron scattering; hence, Fe_3O_4 appears darker because of higher electron density when compared to ZnO nanoparticles in Fig. 5c.[19] HRTEM shown in Fig. 5e gives a d spacing value of 0.19 nm (Fe_3O_4) and 0.24 nm (ZnO) in the nanocomposite[20] which supports the XRD studies. SAED pattern of core shell nanoparticles is represented in Fig. 5f with an (hkl) value of (101) ZnO and (220) Fe_3O_4 which corresponds to the JCPDS card number of the XRD.[21,22]

BET Studies

For determining the surface properties, the N_2 adsorption-desorption isotherm was analysed and is shown in Fig. 6. Fe_3O_4/ZnO NC shows isotherm

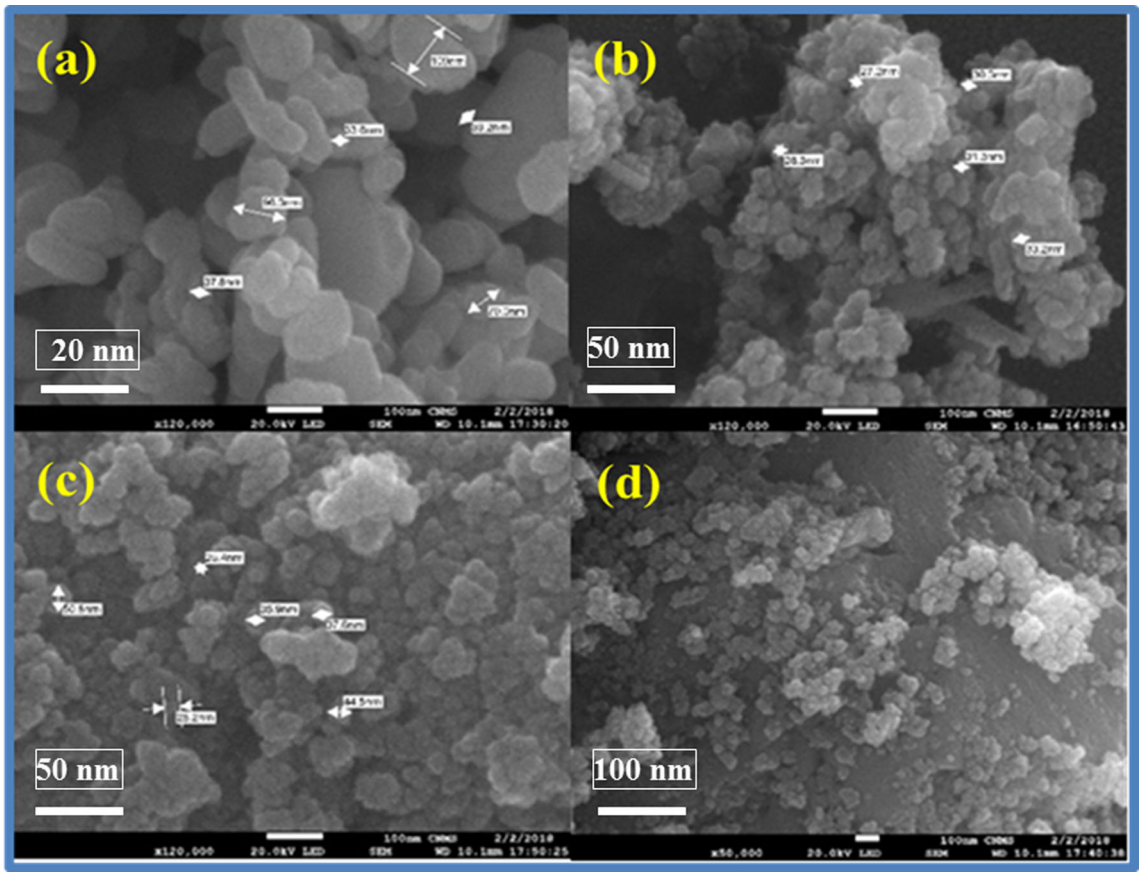

Fig. 3. SEM images of (a) Fe_3O_4, (b) ZnO, (c, d) Fe_3O_4/ZnO NC.

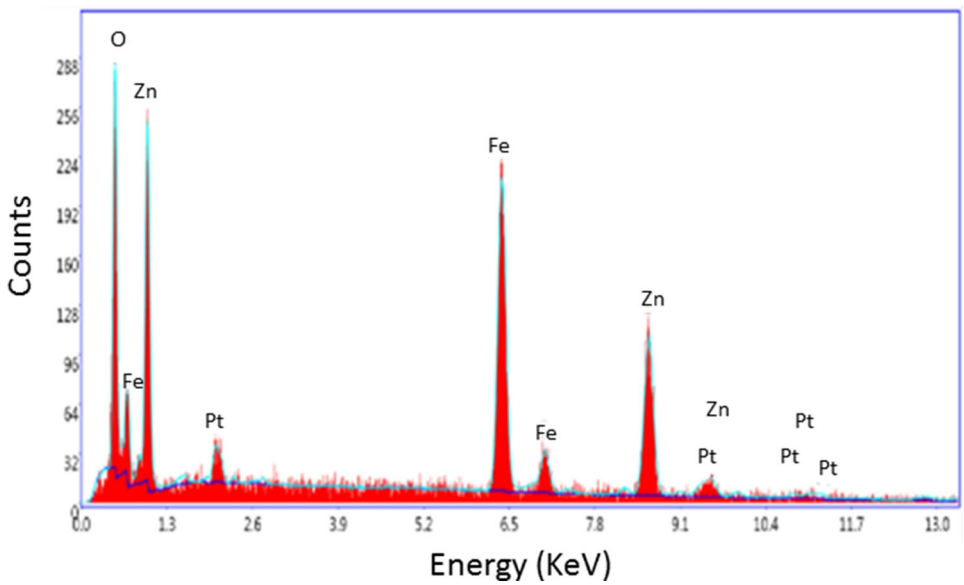

Fig. 4. EDAX analysis of Fe_3O_4/ZnO NC.

hysteresis type (IV). BET surface area, total pore volume and mean pore diameter were found to be 12.647 m^2g^{-1}, 0.024125 cm^3g^{-1} and 7.6302 nm.[23] Because of its high surface area, good pore volume and pore diameter, surface active sites available for the photocatalytic reactions also increases

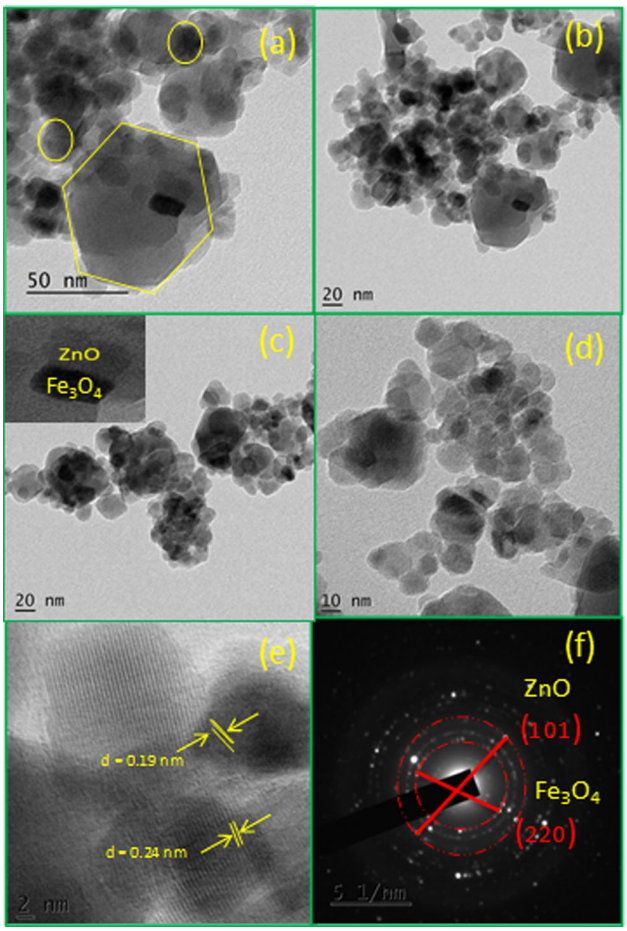

Fig. 5. (a–d) TEM, (e) HRTEM, (f) SAED pattern of Fe_3O_4/ZnO NC.

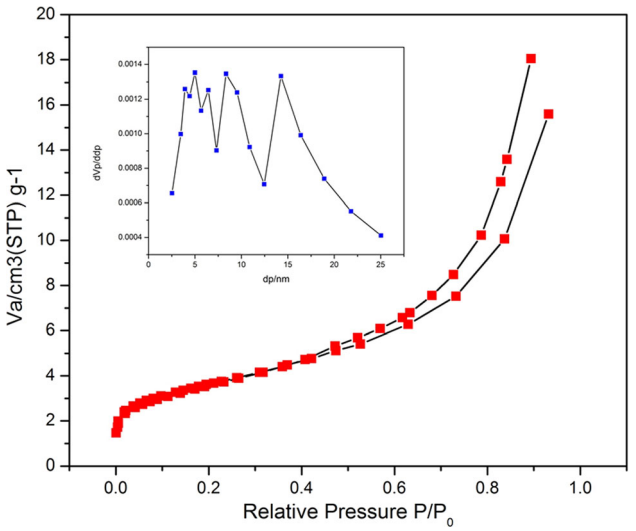

Fig. 6. BET adsorption–desorption isotherm and pore size distribution of Fe_3O_4/ZnO NC.

which slows down the recombination rate of electron hole pairs. In general, high surface area will enhance the catalytic reactions.

UV-Visible DRS Studies

Figure 7a shows the UV-Visible diffused reflectance spectra (DRS) of synthesized Fe_3O_4/ZnO NC. It shows an absorption point at around 464 nm. The Kubelka–Munk (K–M) theory was used to calculate the band gap of Fe_3O_4/ZnO NC, given by the following relation.

$$F(R_\infty) = \frac{1 - R_\infty}{2R_\infty} \tag{2}$$

$$h\nu = \frac{1240}{\lambda} \tag{3}$$

where R_∞ is the reflection coefficient, λ is the absorption wavelength.

For synthesized Fe_3O_4/ZnO NC, the energy gap was found to be around 2.3 eV, as shown in Fig. 7b.[24] Radon et al. found that the optical energy band gap of Fe_3O_4 nanoparticles synthesized by co-precipitation was 3.01 eV. Devi et al. synthesized ZnO nanoparticles by co-precipitation and obtained an energy band gap of 3.30 eV. When compared to these two values in the literature, Fe_3O_4/ZnO NC prepared by co-precipitation in the present work showed a narrow band gap. The obtained band gap of 2.3 eV confirmed that Fe_3O_4/ZnO nanocomposite is a visible active material.[25,26]

Photocatalytic Activity

Figure 8 shows the photocatalytic degradation of Fe_3O_4/ZnO NC against RB and EB as a targeted pollutant under UV light illumination. The decolonization of RB and EB dyes over ZnO, Fe_3O_4 and Fe_3O_4/ZnO NC was recorded by UV-Visible spectroscopy. Before irradiation, the solution mixture was kept in the dark to obtain adsorption/desorption equilibrium. Initially, there were no changes observed for either dye, but after irradiation, it shows that the dye undergoes degradation. The comparison of Fe_3O_4, ZnO and Fe_3O_4/ZnO NC using both RB and EB dyes was carried out. Fe_3O_4/ZnO NC shows 9% degradation at 30 min and 99% degradation at 150 min using RB as a dye, but in EB at 30 min it shows 43% degradation and at 150 min 90% degradation was observed. In RB dye Fe_3O_4/ZnO NC shows the maximum degradation but ZnO has degraded well compared to Fe_3O_4 which is shown in Fig. 8b. Comparison of degradation activity of Fe_3O_4, ZnO, Fe_3O_4/ZnO NC using EB dye is Fe_3O_4/ZnO NC > Fe_3O_4 > ZnO (Fig. 8d).[9,21,23]. The comparative study of degradation of dyes in the presence of ZnO, Fe_3O_4, Fe_3O_4/ZnO NC against RB is shown in Table I.

Mechanism of Photocatalytic Degradation

Photocatalytic degradation of RB and EB dye under UV light illumination using Fe_3O_4/ZnO NC is represented in the following reaction mechanism.

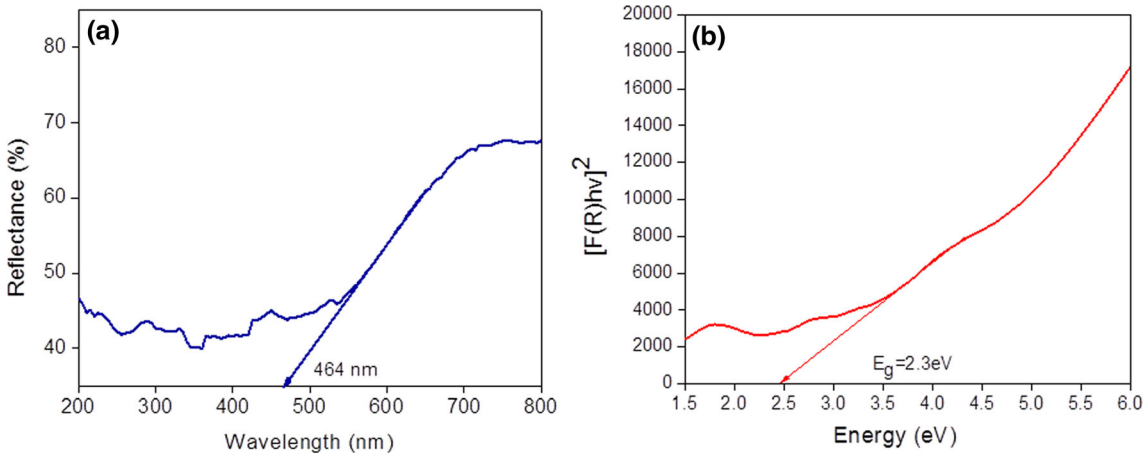

Fig. 7. (a) Diffuse reflectance spectra and (b) direct band gap energy of Fe_3O_4/ZnO NC.

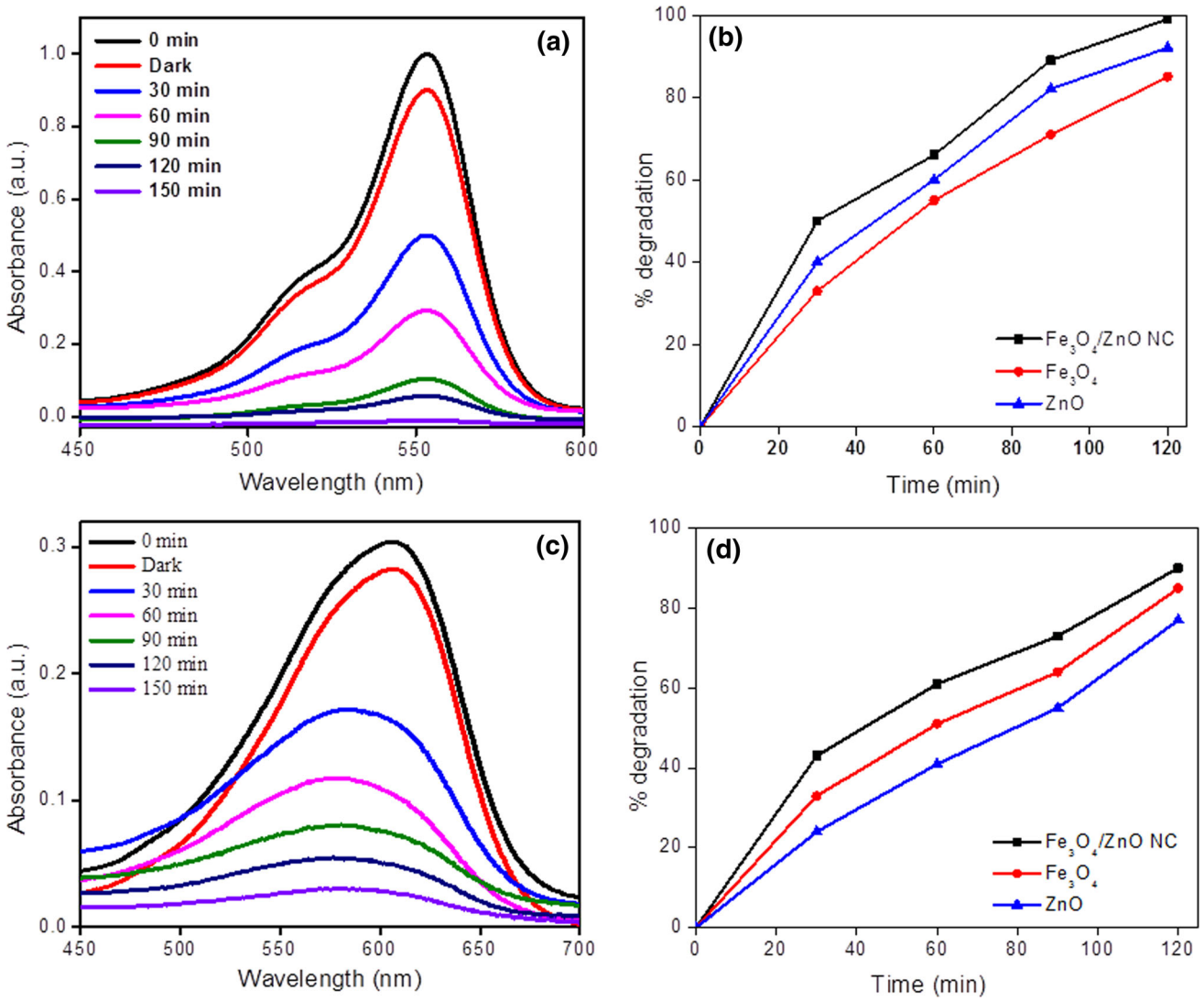

Fig. 8. (a, c) Degradation spectra RhB and EB (b, d) Control experiments over photocatalytic degradation of RhB and EB in the presence of ZnO, Fe_3O_4 and Fe_3O_4/ZnO NC.

Table I. Comparative studies of photocatalytic degradation of RB using ZnO, Fe_3O_4, Fe_3O_4/ZnO NC

Sample no.	Synthesis method	Name of the organic dye	Light source	Degradation (%)	Irradiation time (min)	References
ZnO NPs						
1	Solution phase approach	Rhodamine-B	UV	95	70	29
2	Reflux	Rhodamine-B	UV	100	300	30
3	Hydrothermal	Rhodamine-B	UV	77	50	31
4	Chemical precipitation	Rhodamine-B	UV	100	25	32
5	Co-precipitation	Rhodamine-B	UV	95	150	PW
Fe_3O_4 NPs						
6	Co-precipitation	Rhodamine-B	Visible	98	120	33
7	Co-precipitation	Rhodamine-B	UV	91	150	PW
Fe_3O_4/ZnO NC						
8	Solution combustion	Rhodamine-B	Visible	90	300	34
9	Reverse micelle	Rhodamine-B	Visible	99	40	35
10	Co precipitation	Rhodamine-B	Solar	60	150	36
11	Co-precipitation	Rhodamine-B	UV	99	150	PW

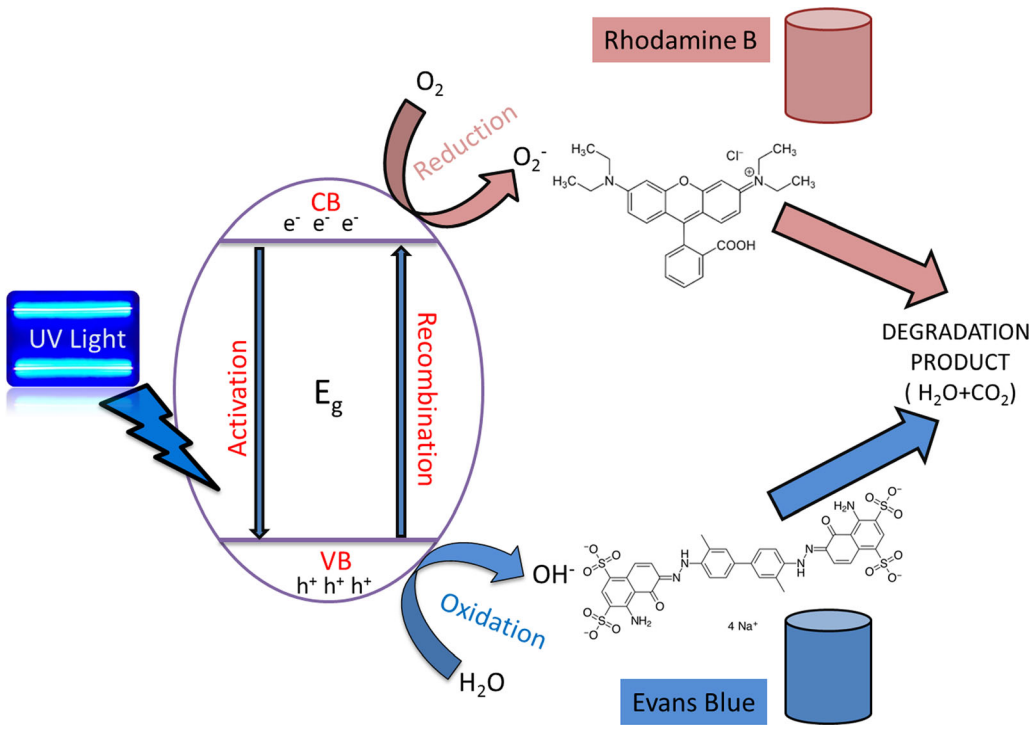

Scheme 2. Mechanism of dye degradation in the presence of Fe_3O_4/ZnO NC under UV light.

$$Fe_3O_4/ZnO + h\nu \rightarrow Fe_3O_4/ZnO\ (h^+_{vb} + e^-_{cb}) \quad (4)$$

$$OH^-_{ads} + h^+_{vb} \rightarrow OH^{\cdot}_{ads}(\text{in basic medium}) \quad (5)$$

$$EB/RB + OH^{\cdot}_{ads} \rightarrow \text{Dye degradation} \quad (6)$$

The schematic representation of the photodegradation of RB and EB using Fe_3O_4/ZnO NC under UV light is shown in Scheme 2. The photodegradation was initiated only when the Fe_3O_4/ZnO NC photocatalyst interacted with the UV light irradiation, the arrangement of e^- (electrons) in conduction band CB and h^+ (holes) in the valence band VB takes place during photoexcitation. To generate anionic superoxide radical ($^{\cdot}O_2^-$) by reduction, the photogenerated electron in the CB reacts with molecular oxygen. e^- gets attracted to the photogenerated hole in VB from hydroxyl ions or water

molecule to yield the most reactive hydroxyl radical ($^{\cdot}OH$) over oxidation. The H_2O_2 generated by reacting with superoxide anion radical with e^-/h^+ pairs. On the surface of Fe_3O_4/ZnO NC, the organic molecules are attacked by these reactive species which act as strong oxidizing agents. Hence, these organic dye molecules easily attacked by ions leads to byproducts. This process is called a redox reaction on the surface of the photocatalyst by the excitation of the catalyst.

Photoluminescence Spectra

To observe the recombination efficiency of generated hole and electron pairs, photoluminescence (PL) spectra was used and is shown in Fig. 9. As depicted in Fig. 9, the intensity of peaks is different which is due to the varying recombination behavior of charge carriers for different materials. PL of Fe_3O_4, Fe_3O_4/ZnO NC, and ZnO NPs were recorded at room temperature. The excitation peak shown at 238 nm was observed at emission peaks of 284 and 392 nm.[9,17,27,28] Photocatalytic activity of a semiconductor photocatalyst is majorly depending on electron and hole. The effect of photocatalytic activity reduces when both the electron and hole recombine to emit a photon. Hence, the lower PL intensity shows the higher photocatalytic activity. The PL of Fe_3O_4/ZnO NC shows the lowest intensity peak when compared to Fe_3O_4 and ZnO. Therefore, photocatalytic performance of Fe_3O_4/ZnO NC is higher than pure Fe_3O_4 and ZnO. Figure 10 shows the X and Y colour coordinates and is known as the CIE (Commission International De I'Eclairage) diagram. From the above figure, the colour of the emitted light from the Fe_3O_4/ZnO NC can be observed and was found to be in the blue region.

Antibacterial Activity

Antibacterial activity of all the three materials was examined against pathogenic bacterial strains such as *Escherichia coli* and *Staphylococcus aureus* by agar well diffusion. The zone of inhibition of prepared NPs with varying concentration of ZnO, Fe_3O_4, Fe_3O_4/ZnO NC (150, 300 and 450 μg/well) with respect to the positive control (ciprofloxacin) was recorded. The results with respect to zone of inhibition were estimated with vernier calipers in millimeters, and its values are shown in Table II where we can observe that the bacterial activity of Fe_3O_4/ZnO is greater when compared to Fe_3O_4 and ZnO individually. This result also indicates that the bacterial activity is completely concentration dependent on the significant effect of nanoparticles against pathogenic bacterial strains. The Fe_3O_4/ZnO NC shows highly significant antibacterial activity against pathogenic strains such as *Escherichia coli* and *Staphylococcus aureus* strains as shown in the Fig. 11. The mechanism for the antibacterial activity of Fe_3O_4/ZnO NC is shown in

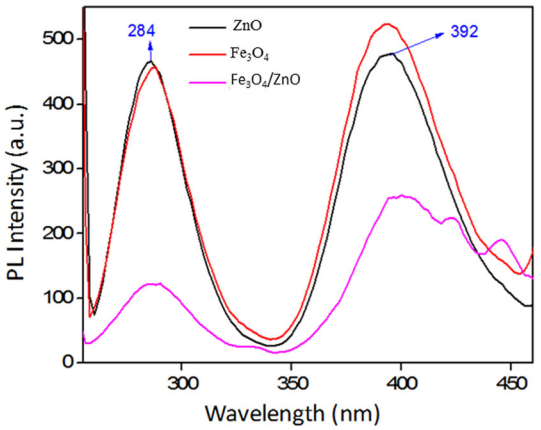

Fig. 9. Photoluminescence spectra of Fe_3O_4/ZnO NC.

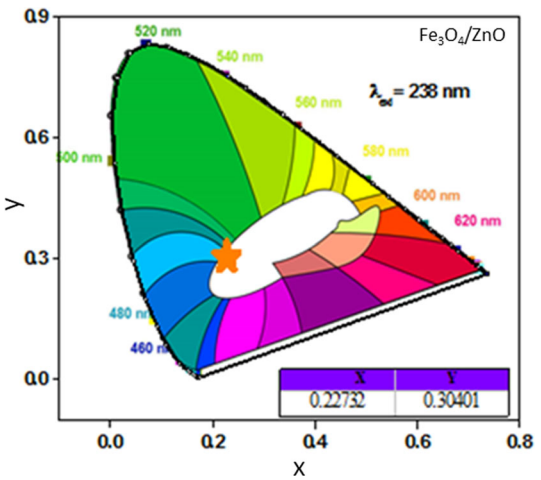

Fig. 10. CIE diagram of synthesized Fe_3O_4/ZnO NC.

Scheme 3.[37,38] The ROS (reactive oxygen species) and release of heavy metal ions, i.e. iron and zinc, were remarkably effective, where these two metals are active sites releasing hydroxide and super oxide radicles which act on the bacteria. Hence, this is the major reason for effective role of Fe_3O_4/ZnO NC, whereas in Fe_3O_4 and ZnO NPs individually have a single metal and less reactive oxygen species when compared to the composite[39,40] where the light irradiation leads to oxidative stress in the cell membrane of the bacteria which finally leads to the death of the bacterial cell. The bacterial death due to the smaller particle size provides larger surface for the interaction with the bacteria which results in effective antibacterial activity. The opposite charge of the prepared nanoparticles and the cell membrane mutually attracts and the Fe_3O_4/ZnO NC enters the bacterial cell membrane reacts with thr thiol group (-SH) present on the surface of the cell which finally leads to the death of the bacterial cell. The comparative study of antibacterial activity in the presence of ZnO, Fe_3O_4, Fe_3O_4/ZnO NC against pathogenic strains is shown in the Table III.

Table II. Antibacterial activity of different Nanoparticles against pathogenic bacterial strains

Sample	Treatment (concentration)	*Escherichia coli* (Mean ± SE)	*Staphylococcus aureus* (Mean ± SE)
Ciprofloxacin	(5 μg/μL)	7.70 ± 0.06	7.03 ± 0.03
ZnO NPs	(a=150 μg/μL)	0.50 ± 0.00	0.50 ± 0.09
	(b=300 μg/μL)	1.17 ± 0.03	1.40 ± 0.06
	(c=450 μg/μL)	3.13 ± 0.09	2.53 ± 0.09
Fe_3O_4	(a=150 μg/μL)	1.13 ± 0.33	1.40 ± 0.06
	(b=300 μg/μL)	2.17 ± 0.07	2.13 ± 0.33
	(c=450 μg/μL)	3.17 ± 0.07	3.40 ± 0.06
Fe_3O_4/ZnO NC	(a=150 μg/μL)	–	–
	(b=300 μg/μL)	1.17 ± 0.07	1.13 ± 0.03
	(c=450 μg/μL)	3.57 ± 0.07	3.97 ± 0.07

Values are the mean ± SE of the zone of inhibition in mm.

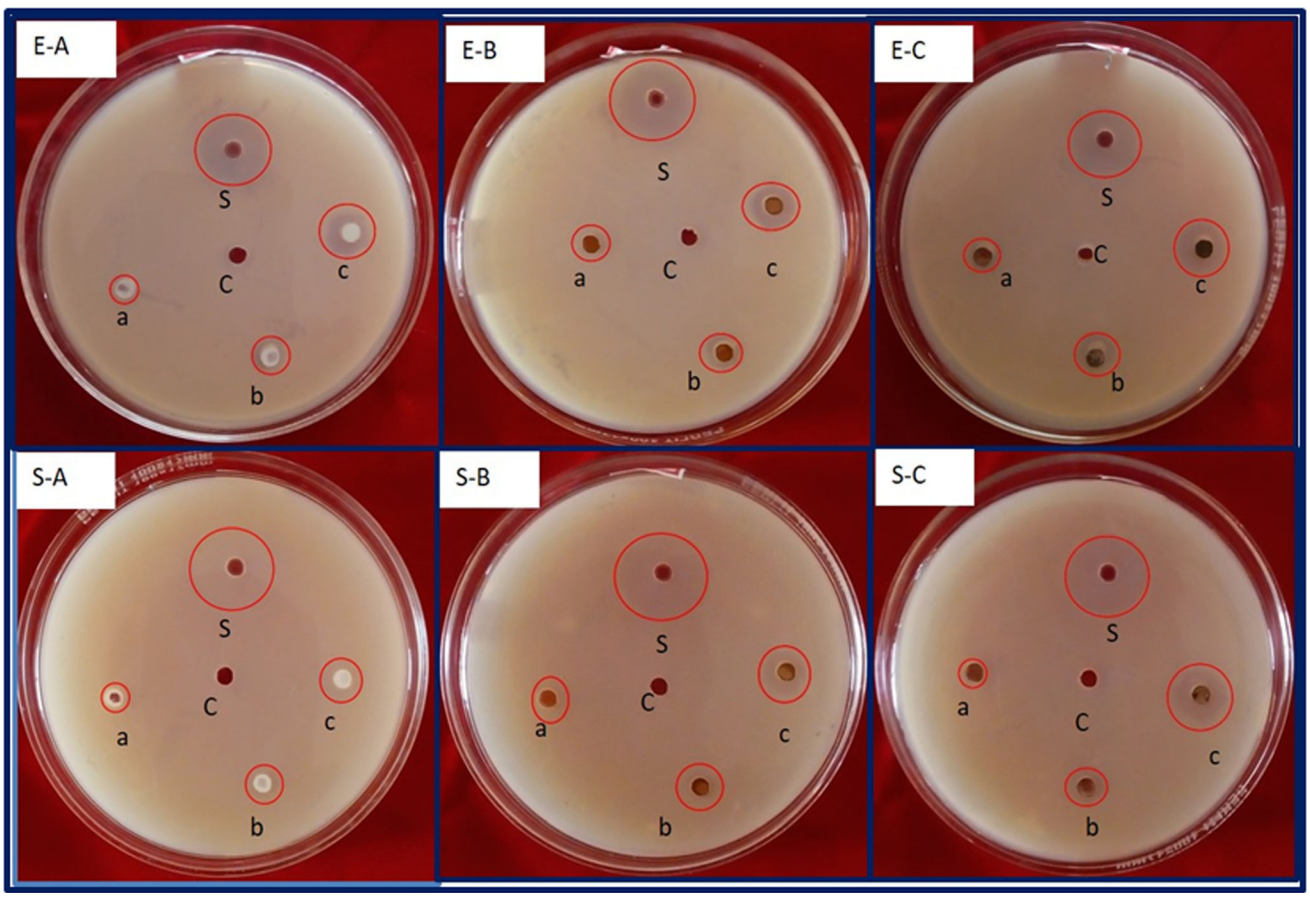

Fig. 11. Show the antibacterial activity of different nanoparticles against pathogenic bacterial strains such as *Escherichia coli* (E-A: ZnO NPs, E-B-Fe_3O_4NPs, E-C= Fe_3O_4/ZnO NC and *Staphylococcus aureus* (S-A: ZnO NPs, S-B-Fe_3O_4 NPs, S-C= Fe_3O_4/ZnO NC).

CONCLUSION

Fe_3O_4@ZnO core-shell NPs were successfully prepared by co-precipitation and were characterized by XRD, FTIR, SEM with EDAX, TEM, BET and UV-Visible spectroscopy. The XRD pattern confirms the formation of Fe_3O_4/ZnO NC by comparing it with Fe_3O_4 and ZnO patterns. Flake- and grain-like morphology was observed in SEM and TEM micrographs. The vibrational modes and M-O bonding confirm the formation of Fe_3O_4/ZnO NC. BET

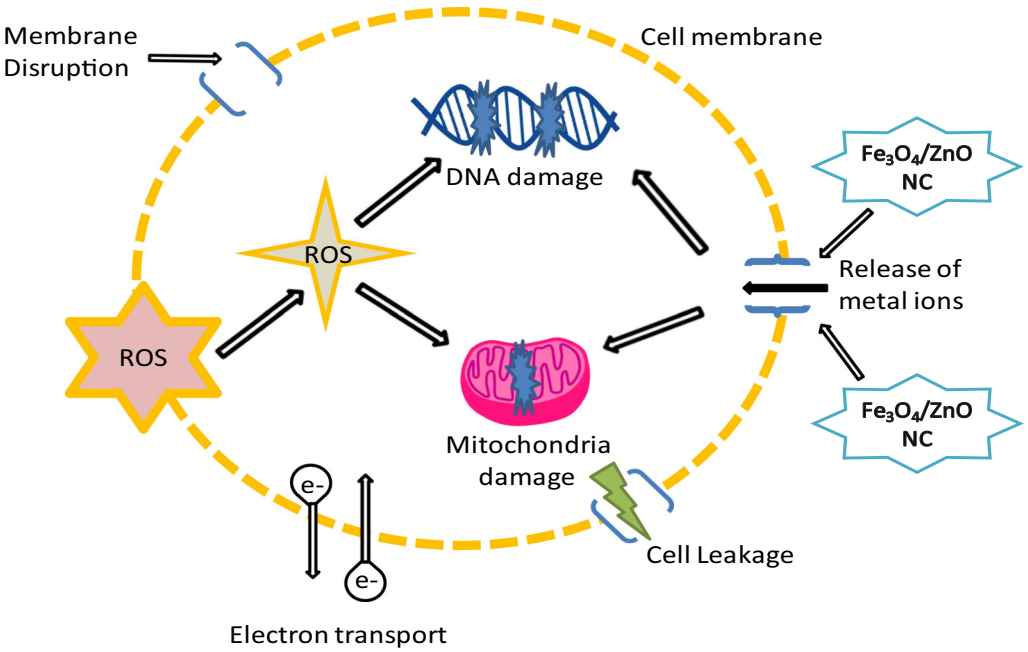

Scheme 3. Mechanism of antibacterial activity of Fe_3O_4/ZnO NC.

Table III. Comparative studies of antibacterial activity using ZnO, Fe_3O_4, Fe_3O_4/ZnO NC

Sample No.	Synthesis method	Bacterial strain tested	Zone of Inhibition (mm)	References
ZnO NPs				
1	Biosynthesis	*Escherichia coli*	1.2 ± 0.02	39
		Staphylococcus aureus	2.4 ± 0.08	
2	Co-precipitation	*Escherichia coli*	3.13 ± 0.09	PW
		Staphylococcus aureus	2.53 ± 0.09	
Fe_3O_4 NPs				
3	Combustion	*Escherichia coli*	2.00 ± 0.02	40
		Staphylococcus aureus	1.4 ± 0.06	
4	Co-precipitation	*Escherichia coli*	3.17 ± 0.07	PW
		Staphylococcus aureus	3.40 ± 0.06	
Fe_3O_4/ZnO NC				
5	Refluxing	*Escherichia coli*	1.22	41
		Staphylococcus aureus		
6	Co-precipitation	*Escherichia coli*	3.57 ± 0.07	PW
		Staphylococcus aureus	3.97 ± 0.07	

analysis shows the surface area of 12.6 m^2g^{-1}. The bang gap was observed at 2.3 eV from UV DRS which is visible active material. From the PL spectra; Fe_3O_4/ZnO NC is useful for optoelectronic applications. The prepared Fe_3O_4/ZnO NC shows significant photocatalytic activity for the degradation of Evans blue and Rhodamine B dyes. The antibacterial activity of Fe_3O_4/ZnO NC demonstrated effective bactericidal activity against gram positive and gram negative bacterial strains. These results show that the prepared Fe_3O_4/ZnO NC synthesis is a very simple, eco-friendly and cost-effective material. It offers potential applications in the field biomedical applications and Fe_3O_4/ZnO nanocomposite is visible active material where amount of visible rays in sun light is around 42% hence Fe_3O_4/ZnO nanocomposite shows possible application in waste water treatment.

ACKNOWLEDGMENTS

M. Shashank thanks Kuvempu University, Shivamogga, Siddaganga Institute of Technology, Tumkur and CNMS, Jain University, for constant support and encouragement. One of the authors Nagaraju Ganganagappa thanks DST Nanomission, Govt. of India, New Delhi (Project No. SR/NM/NS-

1262/2013 dated 18-03-2015) and VGST, Govt. of Karnataka (VGST/SMYSR/2015-2016//GRD-498) for financial support to carry out the research work. Dr. M. Madhukara Naik thanks the Principal and the Management for supporting the research activity.

CONFLICT OF INTEREST

The authors declared that they have no conflict of interest.

REFERENCES

1. R. Saravanan, S. Karthikeyan, V.K. Gupta, G. Sekaran, V. Narayanan, and A.J.M.S. Stephen, *Mater. Sci. Eng., C* 33, 91 (2013).
2. K. Karthik, S. Dhanuskodi, C. Gobinath, S. Prabukumar, and S. Sivaramakrishnan, *J. Mater. Sci.: Mater. Electron.* 29, 5459 (2018).
3. R.Y. Hong, J.H. Li, L.L. Chen, D.Q. Liu, H.Z. Li, Y. Zheng, and J. Ding, *Powder Technol.* 189, 426 (2009).
4. J. Xia, A. Wang, X. Liu, and Z. Su, *Appl. Surf. Sci.* 257, 9724 (2011).
5. Q.L. Feng, J. Wu, G.Q. Chen, F.Z. Cui, T.N. Kim, and J.O. Kim, *J. Biomed. Mater. Res.* 52, 662 (2000).
6. J. Saffari, N. Mir, D. Ghanbari, K. Khandan-Barani, A. Hassanabadi, and M.R. Hosseini-Tabatabaei, *J. Mater. Sci.: Mater. Electron.* 26, 9591 (2015).
7. J. Sun, H. Fan, B. Nan, and S. Ai, *Sep. Purif. Technol.* 130, 84 (2014).
8. S. Aslam, J. Zeng, F. Subhan, M. Li, F. Lyu, Y. Li, and Z. Yan, *J. Colloid Interface Sci.* 505, 186 (2017).
9. J. Wang, J. Yang, X. Li, D. Wang, B. Wei, H. Song, X. Li, and S. Fu, *Physica E* 75, 66 (2016).
10. S.K. Rajabi, and S.H. Sohrabnezhad, *Microporous Mesoporous Mater.* 242, 136 (2017).
11. J. Wan, H. Li, and K. Chen, *Mater. Chem. Phys.* 114, 30 (2009).
12. M.M. Naik, H.S.B. Naik, G. Nagaraju, M. Vinuth, K. Vinu, and S.K. Rashmi, *J. Mater. Sci.: Mater. Electron.* 29, 20395 (2018).
13. C. Perez, *Acta Biol. Med. Exp.* 15, 113 (1990).
14. X. Sun, G. Ma, X. Lv, M. Sui, H. Li, F. Wu, and J. Wang, *Materials* 11, 780 (2018).
15. S.D. Kulkarni, S.M. Kumbar, S.G. Menon, K.S. Choudhari, and C. Santhosh, *Adv. Sci. Lett.* 23, 1724 (2017).
16. C. Karunakaran, and P. Vinayagamoorthy, *New J. Chem.* 40, 1845 (2016).
17. R.Y. Hong, S.Z. Zhang, G.Q. Di, H.Z. Li, Y. Zheng, J. Ding, and D.G. Wei, *Mater. Res. Bull.* 43, 2457 (2008).
18. X. Huang, J. Lu, D. Yue, Y. Fan, C. Yi, X. Wang, M. Zhang, and J. Pan, *Nanotechnology* 26, 125101 (2015).
19. V. Madhubala, and T. Kalaivani, *Appl. Surf. Sci.* 449, 584 (2018).
20. Y.-J. Chen, F. Zhang, G.-G. Zhao, X.-Y. Fang, H.-B. Jin, P. Gao, C.-L. Zhu, M.-S. Cao, and G. Xiao, *J. Phys. Chem. C* 114, 9239 (2010).
21. M. Dehghani-Dashtabi, H. Hekmatara, and J. Seyed-Yazdi, *Phys. B* 553, 11 (2019).
22. C. Karunakaran, P. Vinayagamoorthy, and J. Jayabharathi, *Langmuir* 30, 15031 (2014).
23. V. Panwar, P. Kumar, A. Bansal, S.S. Ray, and S.L. Jain, *Appl. Catal. A* 498, 25 (2015).
24. X. Zhang, J. Wu, G. Meng, X. Guo, C. Liu, and Z. Liu, *Appl. Surf. Sci.* 366, 486 (2016).
25. A. Radoń, A. Drygała, Ł Hawełek, and D. Łukowiec, *Mater. Charact.* 131, 148 (2017).
26. P.G. Devi, and A.S. Velu, *J. Theor. Appl. Phys.* 10, 223 (2016).
27. S. Chidambaram, B. Pari, N. Kasi, and S. Muthusamy, *J. Alloy Compd.* 665, 404 (2016).
28. J.C.B. Huarac, M.S. Tomar, S.P. Singh, O. Perales-Perez, L. Rivera, and S. Pena, *InNSTI-Nanotech.* 3, 405 (2010).
29. Q.I. Rahman, M. Ahmad, S.K. Misra, and M. Lohani, *Mater. Lett.* 91, 170 (2013).
30. O.S. Bello, K.A. Adegoke, S.O. Fagbenro, and O.S. Lameed, *Appl. Water Sci.* 9, 189 (2019).
31. Y. Lai, M. Meng, Y. Yu, X. Wang, and T. Ding, *Appl. Catal. B* 105, 335 (2011).
32. J. Zhai, X. Tao, Y. Pu, X.-F. Zeng, and J.-F. Chen, *Appl. Surf. Sci.* 257, 393 (2010).
33. C.-C. Lin, and J.-M. Ho, *Ceram. Int.* 40, 10275 (2014).
34. S. Sun, X. Yang, Y. Zhang, F. Zhang, J. Ding, J. Bao, and C. Gao, *Prog. Nat. Sci.: Mater. Int.* 22, 639 (2012).
35. C. Singh, S. Jauhar, V. Kumar, J. Singh, and S. Singhal, *Mater. Chem. Phys.* 156, 188 (2015).
36. X. Cao, L. Gu, X. Lan, C. Zhao, D. Yao, and W. Sheng, *Mater. Chem. Phys.* 106, 175 (2007).
37. M.M. Naik, H.S.B. Naik, N. Kottam, M. Vinuth, G. Nagaraju, and M.C. Prabhakara, *J. Sol-Gel. Sci. Technol.* 91, 578 (2019).
38. M.M. Naik, H.S.B. Naik, G. Nagaraju, M. Vinuth, K. Vinu, and R. Viswanath, *Nano-Struct. Nano-Objects* 19, 100322 (2019).
39. C. Jayaseelan, A.A. Rahuman, A.V. Kirthi, S. Marimuthu, T. Santhoshkumar, A. Bagavan, K. Gaurav, L. Karthik, and K.V.B. Rao, *Spectrochim. Acta Part A Mol. Biomol. Spectrosc.* 90, 78 (2012).
40. Y.T. Prabhu, K.V. Rao, B.S. Kumari, V.S.S. Kumar, and T. Pavani, *Int. Nano Lett.* 5, 85 (2015).
41. S. Singh, K.C. Barick, and D. Bahadur, *Powder Technol.* 269, 513 (2015).